Journal of Cleaner Production 193 (2018) 277–289

Contents lists available at ScienceDirect

Journal of Cleaner Production

journal homepage: www.elsevier.com/locate/jclepro

Physical properties optimization of POME-groundnut-naphthenic based graphene nanolubricant using response surface methodology

Mohamed Osama [a], Rashmi Walvekar [a, **], Mohammad Khalid [b, *], Abdul Khaliq Rasheed [b], Wai Yin Wong [c], Thummalapalli Chandra Sekhara Manikyam Gupta [d]

[a] School of Engineering, Taylor's University Lakeside Campus, Subang Jaya, Malaysia
[b] Graphene & Advanced 2D Materials Research Group (GAMRG), School of Science and Technology, Sunway University, No. 5, Jalan Universiti, Bandar Sunway, 47500, Subang Jaya, Selangor, Malaysia
[c] Fuel Cell Institute, Universiti Kebangsaan Malaysia, Bangi, Selangor, Malaysia
[d] Research and Development, Apar Industries Limited, Mumbai, India

ARTICLE INFO

Article history:
Received 4 July 2017
Received in revised form
26 April 2018
Accepted 8 May 2018
Available online 9 May 2018

Keywords:
Naphthenic
Groundnut
POME
Graphene
Nanofluid
Optimization

ABSTRACT

In this research, different oil blends were produced by mixing naphthenic base oil, groundnut oil, palm oil methyl ester and nanometer thick graphene flakes. The thermophysical properties such as viscosity, thermal conductivity, volatility and suspension stabilities were measured and modeled for each oil and blends. Every individual parameter was modeled following quadratic multiple linear regression analysis and optimized using the desirability approach. The behavior of each selected property as a function of groundnut oil, palm oil methyl ester and graphene concentrations are discussed and consequently optimized to select the best combination of constituents. While groundnut oil, palm oil methyl ester and graphene were used as additives, had various effects independently on the property of naphthenic base oil. The first noteworthy observation is that the blends made with the higher composition of groundnut oil resulted in higher viscosity index, thermal conductivity, nanosuspension stability, and reduced volatility. Secondly, the viscosity index and thermal conductivity of graphene-based groundnut oil compared to pure naphthenic oil enhanced by 49% and 38% respectively. On the other hand, its stability and volatility reduced by 79% and 98% respectively. Thirdly, palm oil methyl ester as an additive was found to be less effective as the groundnut oil composition was increased. Overall, the results of this study show that groundnut oil, palm oil methyl ester and graphene could make excellent metalworking fluids and additives in different combinations.

1. Introduction

Generally, metalworking operations involve high pressure, temperature, friction and wear. During metalworking operations, lubricants assist in heat and chip removal, surface finish and prevent thermal deformation of the workpiece (Van Der Heide and Schipper, 2006; Rizvi, 2009). Manufacturing is an important economic sector for many countries. For instance, in the United States, about one-eighth of the gross domestic product is held by the manufacturing industries (Groover, 2010). Therefore, research and development of new efficient cutting fluids are highly essential in order to maintain strong and competent manufacturing base. The majority of modern lubricants are low-cost mineral oils, however, their disposal is a concern as they pollute the environment (Van Der Heide and Schipper, 2006). Mineral oils are classified as paraffinic, naphthenic or aromatic. Among these, the naphthenic type has average thermophysical properties between the two extremes. For instance, naphthenic structures have an inferior viscosity-temperature behavior when compared to paraffinic structures, but at the same time superior to aromatics. Therefore, naphthenic structures are preferred in metalworking operations (Van Der Heide and Schipper, 2006).

Due to growing environmental regulations, the demand for biodegradable lubricants has increased. In fact, it has been reported that more than 50% of the sold lubricants pollute the environment through spillage, evaporation and total-loss lubrication (Joseph

* Corresponding author.
** Corresponding author.
E-mail addresses: RashmiGangasa.Walvekar@taylors.edu.my (R. Walvekar), khalids@sunway.edu.my (M. Khalid).

https://doi.org/10.1016/j.jclepro.2018.05.070
0959-6526/

et al., 2013). On the other hand, vegetable oils and animal fats are biodegradable and therefore their disposal is of a lesser concern. Moreover, vegetable oils are non-toxic and non-carcinogenic as well. Applications of vegetable oils to the metalworking operations have been reported to improve the machining performance by many researchers (Lawal et al., 2012). For example, groundnut oil as a metalworking fluid showed superior performance in two different studies. Ojolo et al. (2008) investigated the effects of four straight biological oils on the cutting force during cylindrical turning. In their study, groundnut oil exhibited the highest reduction of the cutting force relative to palm kernel, coconut and shea butter oils. In another study, Lawal et al. (2007) studied the performance of a commercial cutting fluid that was compared with groundnut, palm and palm kernel oils. It was found that groundnut oil performed as the best coolant at all the experimented speeds. However, a number of disadvantages associated with vegetable oils are related to their poor oxidative stability and low-temperature properties. Therefore, vegetable oil properties are enhanced by chemically modifying their structures. Transesterification process is widely used to produce alternatives to vegetable oils such as palm oil methyl ester (POME) (Khalid and Khalid, 2011). It has been reported that the sulfur content of POME is about 0.002 wt% making it environmentally friendly. Further, the addition of POME to coolants in quantities as small as 5 vol%, resulted in lower steady-state friction coefficient (Dayou et al., 2011). Furthermore, the occurrence of fracture and cracking was delayed during the milling operation.

Relative to biological oils, there is a growing interest in the use of nanoparticles as additives. Nanoparticles have the advantage of small size which enables them to enter surfaces in contact at micro-nano level (Mansot et al., 2008), resulting in better performance. Graphene, which is commonly referred as nanosheets and nanoflakes owing to its nanometer thickness (Li et al., 2008; Han et al., 2016; Thirumalraj et al., 2017), has been reported to slow down the corrosive and oxidative processes that cause damage to the rubbing surfaces (Berman et al., 2014), resulting in higher tool life. Graphene having a thermal conductivity in the range of 2000–4000 W m^{-1} K^{-1} (Pop et al., 2012) could play a great role in heat dissipation during the machining process. Graphene dispersed in oils and coolants popularly known as nanofluids and nanolubricants (Rasheed et al., 2016; Sadeghinezhad et al., 2016), have been reported to offer enhanced tribological properties. For instance, Lin et al., showed that the modified graphene platelets at an optimum concentration of 0.075 wt% was able to improve the load carrying capacity (Lin et al., 2011). In another study, Agostino et al. reported that graphene oxide additives reduced the coefficient of friction by more than 20% (D'Agostino et al., 2012). Rashmi et al., analyzed the tribological properties of graphene-based palm oil trimethylolpropane nanofluid (Rashmi et al., 2017). The results indicate that 0.05 wt% graphene nanoflakes reduced the frictional coefficient by 7% and the wear scar diameter by 16.2%. Nevertheless, graphene remains a non-degradable constituent and its addition to biological oils might dispute the overall biodegradability of biological oils. Interestingly, Sridhar et al. showed that graphene had a marginal effect on the overall biodegradability of PHBV polymer (Sridhar et al., 2012). This result could be also true for oil-based nanofluids, especially due to the fact that graphene nanoparticles are to be dispersed at very small weight fractions. Despite these promising findings, the use of graphene remains critical due to its toxicity and risks to living organisms. Nonetheless, several studies showed that graphene could be biodegraded by microbes and enzymes (Chen et al., 2017). Thus, the toxic effect of graphene on the environment could be managed and mitigated.

From the literature, it can be deduced that the majority of optimization studies on cutting fluids focused on selecting the best-cutting fluid in terms of how closely it satisfies response-based target, minimum or maximum criteria for cutting process parameters with little or no regard to optimizing formulation based on responses of physical properties. For instance, studies such as in Kuram et al. (2010) and Do and Hsu (2016) determined the best formulation or base fluid based on examining cutting process parameters. On the other hand, Muniz et al., 2008 focused on optimizing cutting fluid formulation based on the response of selected physical properties. Very few reports addressed nanosuspension (nanofluid) stabilities of the tested cutting fluids throughout the literature. In this paper, the main focus is to optimize the formulation of novel cutting fluids by examining selected physical properties and nanosuspension stabilities. Such optimization can provide a meaningful and feasible method to narrow down cutting fluid samples for further thorough cutting analysis. Additionally, if the reliable correlation were to be found between physical properties and cutting performance parameters, optimization of cutting fluid formulation based on the response of physical properties can provide alternative and cheaper method to select the optimum formulation or base fluid for targeted cutting applications.

In the present paper, different blends of base fluids are formulated using naphthenic base oil, groundnut oil, POME and graphene nanoflakes at varying concentrations. Different physical properties were measured, calculated and modeled to optimize composition following the desirability approach. The findings of this paper can be used to optimize the composition of the lubricants studied to comply with performance requirements of various lubricating applications.

2. Materials

The naphthenic oil (T 22) was supplied by (Nynas Pte Ltd, Singapore) and POME was supplied by (Excel Vite Sdn Bhd, Malaysia). The groundnut oil was purchased from (Waitrose, United Kingdom). The graphene nanoflakes were purchased from (Graphene Supermarket, United States). The average thickness of graphene nanoflakes is 60 nm with a purity of about 98.5% and average lateral size is ≤ 7 μm. The specific surface area of the graphene nanoflakes is smaller than or equal to 40 m^2/g.

3. Experimental methodology

3.1. Samples formulation

In this research, we describe the nanometer thick graphene based oil blend as nanolubricant. The samples were prepared by mixing naphthenic base oil, groundnut oil, POME and graphene nanoflakes at different proportions and concentrations. In order to study the effect of POME, three different concentrations (3 vol%, 5 vol% and 7 vol%) were studied. Similarly, the effect of graphene was studied at three different concentrations (0.075 wt%, 0.1 wt% and 0.125 wt%). The groundnut oil was used at five levels to examine different combinations of the naphthenic-groundnut oil blend. Groundnut oil was examined at concentrations of 25 wt%, 50 wt%, 75 wt% and 100 wt%. The pure naphthenic oils were prepared at the different composition of POME and graphene nanoflakes. The graphene-based nanolubricant were prepared by dispersing graphene nanoflakes using water bath ultrasonicator (iLab Equipment). Rashmi et al., reported that the optimum sonication duration for CNT based water nanofluid is 4 h (Rashmi et al., 2011). Chang et al. and Nurdin et al. showed that the temperature

Table 1
Composition of different samples.

Sample Run	Sample Label	Constituents			
		Mineral (wt %)	Groundnut (wt %)	POME (vol %)	Graphene (wt %)
1	ML	100	0	0	0
2	BML1	75	25	0	0
3	BML2	50	50	0	0
4	BML3	25	75	0	0
5	BL	0	100	0	0
6	PML1	100	0	3	0
7	PML2	100	0	5	0
8	PML3	100	0	7	0
9	PBML1	75	25	3	0
10	PBML2	50	50	3	0
11	PBML3	25	75	3	0
12	PBML4	75	25	5	0
13	PBML5	50	50	5	0
14	PBML6	25	75	5	0
15	PBML7	75	25	7	0
16	PBML8	50	50	7	0
17	PBML9	25	75	7	0
18	PBL1	0	100	3	0
19	PBL2	0	100	5	0
20	PBL3	0	100	7	0
21	GML1	100	0	0	0.075
22	GML2	100	0	0	0.1
23	GML3	100	0	0	0.125
24	GBML1	75	25	0	0.075
25	GBML2	50	50	0	0.075
26	GBML3	25	75	0	0.075
27	GBML4	75	25	0	0.1
28	GBML5	50	50	0	0.1
29	GBML6	25	75	0	0.1
30	GBML7	75	25	0	0.125
31	GBML8	50	50	0	0.125
32	GBML9	25	75	0	0.125
33	GBL1	0	100	0	0.075
34	GBL2	0	100	0	0.1
35	GBL3	0	100	0	0.125
36	GPML1	100	0	3	0.075
37	GPML2	100	0	5	0.075
38	GPML3	100	0	7	0.075
39	GPML4	100	0	3	0.1
40	GPML5	100	0	5	0.1
41	GPML6	100	0	7	0.1
42	GPML7	100	0	3	0.125
43	GPML8	100	0	5	0.125
44	GPML9	100	0	7	0.125
45	GPBML1	75	25	3	0.075
46	GPBML2	50	50	3	0.075
47	GPBML3	25	75	3	0.075
48	GPBML4	75	25	5	0.075
49	GPBML5	50	50	5	0.075
50	GPBML6	25	75	5	0.075
51	GPBML7	75	25	7	0.075
52	GPBML8	50	50	7	0.075
53	GPBML9	25	75	7	0.075
54	GPBML10	75	25	3	0.1
55	GPBML11	50	50	3	0.1
56	GPBML12	25	75	3	0.1
57	GPBML13	75	25	5	0.1
58	GPBML14	50	50	5	0.1
59	GPBML15	25	75	5	0.1
60	GPBML16	75	25	7	0.1
61	GPBML17	50	50	7	0.1
62	GPBML18	25	75	7	0.1
63	GPBML19	75	25	3	0.125
64	GPBML20	50	50	3	0.125
65	GPBML21	25	75	3	0.125
66	GPBML22	75	25	5	0.125
67	GPBML23	50	50	5	0.125
68	GPBML24	25	75	5	0.125
69	GPBML25	75	25	7	0.125
70	GPBML26	50	50	7	0.125
71	GPBML27	25	75	7	0.125
72	GPBL1	0	100	3	0.075
73	GPBL2	0	100	5	0.075
74	GPBL3	0	100	7	0.075
75	GPBL4	0	100	3	0.1
76	GPBL5	0	100	5	0.1
77	GPBL6	0	100	7	0.1
78	GPBL7	0	100	3	0.125
79	GPBL8	0	100	5	0.125
80	GPBL9	0	100	7	0.125

affects the stability of the CuO and Maghemite based nanofluids respectively (Chang et al., 2005; Nurdin et al., 2016). Therefore, the graphene nanoflakes were dispersed following a sonication period of 4 h at intervals of 30 min. The water was changed every 30 min to maintain the bath at room temperature which shall ensure uniformity of dispersion. Table 1 shows the samples involved in the study along with their unique groupings. In Table 1, M represents mineral (naphthenic), B represents bio oil (groundnut), P represents POME and G represents graphene.

3.2. Nanolubricant stability

The stability of the nanodispersion was assessed following qualitative and quantitative methods. The former was performed by capturing images of the nanolubricant samples at different intervals for a period of 1 month to visually observe the nanoflakes sedimentation. The samples were grouped according to their pure and blend parent samples. On the other hand, quantitative stability characteristics of the graphene nanosuspension (0.075–0.125 wt%) were measured using Genesys 10 S UV–vis spectrophotometer from Thermo Scientific. The sedimentation rate was determined by measuring the supernatant concentration of the nanosuspension. The full range spectrum run was used to determine the peak wavelength of graphene nanosuspension in oil and was found to be 225 nm. The absorbance value of each nanosuspension was measured with respect to its base fluid (reference sample). For each base fluid, a unique calibration curve which relates the absorbance to graphene concentration was prepared. Thus, the absorbance of the sample on subsequent days was converted to graphene concentration using the calibration curve. Using this data, the sedimentation rate was computed using Eq (1) and it was used as an indicator for quantitative assessment of the overall stability.

$$SR = \frac{wt_o\% - wt_t\%}{t} \tag{1}$$

3.3. Dynamic viscosity measurements

The dynamic viscosity was measured at temperatures of 24 °C, 40 °C and 100 °C using Haake Mars Rheometer (model: III) from Thermo Scientific. The measurements were carried using titanium plate sensor PP35. About 1 ml of each sample was placed on the plate sensor to carry out the measurements. The viscosity was measured at two different shear rates, 10 s^{-1} and 500 s^{-1}. The average viscosity between these two shear rates was computed and used for further analysis. The dynamic viscosity at a temperature of 40 °C was used for the viscosity model.

Table 2
Experimental results.

Sample	SR (wt%/month)	DV (cP)	VI	TC (W/m.K)	NV (%)
ML	–	22.673	177.80	0.1181	95.34
BML1	–	24.777	210.00	0.1246	–
BML2	–	27.993	238.43	0.1372	46.88
BML3	–	32.908	255.81	0.1463	–
BL	–	38.344	270.70	0.1611	1.66
PML1	–	20.300	189.58	0.1158	93.04
PML2	–	18.616	206.71	0.1193	–
PML3	–	17.700	203.62	0.1168	92.98
PBML1	–	21.802	226.59	0.1264	–
PBML2	–	25.994	236.33	0.1375	47.56
PBML3	–	30.521	252.81	0.1483	–
PBML4	–	20.475	239.84	0.1269	–
PBML5	–	24.554	245.09	0.1378	–
PBML6	–	29.351	259.99	0.1473	–
PBML7	–	19.695	247.58	0.1266	–
PBML8	–	23.663	248.14	0.1370	51.50
PBML9	–	27.161	275.38	0.1505	–
PBL1	–	35.486	276.42	0.1594	3.86
PBL2	–	34.171	277.97	0.1592	–
PBL3	–	32.800	282.89	0.1596	6.71
GML1	0.349	22.304	189.06	0.1159	98.08
GML2	0.543	22.441	183.21	0.1169	–
GML3	0.760	22.275	180.10	0.1175	97.90
GBML1	0.415	24.801	201.03	0.1263	–
GBML2	0.106	28.317	235.77	0.1388	48.43
GBML3	0.052	32.109	259.67	0.1508	–
GBML4	0.580	24.235	224.22	0.1277	–
GBML5	0.260	28.621	236.03	0.1365	–
GBML6	0.244	32.613	256.18	0.1495	–
GBML7	0.757	24.305	221.39	0.1272	–
GBML8	0.419	27.268	245.55	0.1395	48.42
GBML9	0.361	32.123	264.96	0.1499	
GBL1	0.030	37.033	273.82	0.1597	2.20
GBL2	0.111	38.314	268.15	0.1609	–
GBL3	0.387	38.570	272.31	0.1622	1.10
GPML1	0.388	20.642	202.08	0.1165	97.99
GPML2	0.431	19.595	208.05	0.1188	–
GPML3	0.374	17.862	225.02	0.1203	99.56
GPML4	0.607	20.346	197.94	0.1169	–
GPML5	0.574	18.990	213.88	0.1187	–
GPML6	0.552	18.237	210.72	0.1188	–
GPML7	0.722	20.754	191.53	0.1171	97.53
GPML8	0.738	19.972	205.57	0.1179	–
GPML9	0.790	18.741	217.49	0.1187	96.38
GPBML1	0.502	22.065	227.92	0.1253	–
GPBML2	0.227	25.954	249.26	0.1369	50.70
GPBML3	0.093	29.808	268.11	0.1483	–
GPBML4	0.507	20.897	239.60	0.1274	–
GPBML5	0.277	25.148	252.36	0.1385	–
GPBML6	0.073	28.591	272.81	0.1470	–
GPBML7	0.522	19.683	256.69	0.1282	–
GPBML8	0.199	24.649	252.75	0.1382	50.44
GPBML9	0.013	27.147	280.63	0.1481	–
GPBML10	0.688	22.103	234.78	0.1254	–
GPBML11	0.419	25.703	252.20	0.1396	–
GPBML12	0.172	29.926	269.09	0.1503	–
GPBML13	0.679	21.142	243.70	0.1271	–
GPBML14	0.377	25.265	248.97	0.1397	–
GPBML15	0.208	28.459	276.26	0.1499	–
GPBML16	0.683	20.177	249.77	0.1263	–
GPBML17	0.356	23.988	258.07	0.1390	–
GPBML18	0.150	27.402	272.91	0.1464	–
GPBML19	0.824	22.763	226.84	0.1273	–
GPBML20	0.521	25.637	257.85	0.1397	48.74
GPBML21	0.315	29.994	271.12	0.1500	–
GPBML22	0.866	21.652	224.87	0.1291	–
GPBML23	0.548	25.314	252.63	0.1394	–
GPBML24	0.402	28.402	270.30	0.1499	–
GPBML25	0.872	20.542	234.46	0.1274	–
GPBML26	0.506	23.936	257.01	0.1386	50.90
GPBML27	0.339	27.099	274.55	0.1473	–
GPBL1	0.004	34.566	281.94	0.1580	3.12
GPBL2	0.147	33.415	281.45	0.1583	–
GPBL3	0.017	31.750	289.65	0.1621	6.65
GPBL4	0.174	35.797	276.07	0.1598	–
GPBL5	0.212	34.214	277.67	0.1608	–
GPBL6	0.168	32.623	282.09	0.1591	–
GPBL7	0.418	33.875	289.90	0.1613	3.22
GPBL8	0.409	33.070	289.19	0.1586	–
GPBL9	0.326	32.662	289.09	0.1586	7.03

3.4. Viscosity index characterization

The viscosity index was calculated as per ASTM D2270 which determines the viscosity index from the kinematic viscosity at temperatures of 40 °C and 100 °C. In this research, the kinematic viscosity was calculated using the following formula,

$$\nu = \frac{\mu}{\rho} \tag{2}$$

Where ν represents kinematic viscosity, μ dynamic viscosity and ρ density. The density data was determined using Anton Paar (DMA 4500 M) at temperatures of 40 °C and 100 °C. It is to be noted that the viscosity index values were not calculated from standard data (ASTM D 445). As such, the reported results of viscosity index shall be used only for informational purposes and should not be considered desirable for specification purposes.

3.5. Thermal conductivity measurements

The thermal conductivity was measured at temperatures of 25 °C, 40 °C and 55 °C using KD2 Pro thermal property analyzer (Decagon device, USA). The measurements were carried out using single needle KS-1 that was immersed in a test sample from the top. Thermal conductivities were recorded three times for each sample run to obtain an average value. Only consistent readings with an error value below 0.7% are accepted. The average value of the thermal conductivity at different temperatures were calculated and used for subsequent analysis.

3.6. Volatility characterization

The sample evaporation tendencies or the Noack volatilities were assessed as per ASTM D6375. The TGA 8000 instrument from Perkin Elmer was used to carry out the measurements. Synthetic air was used as purge gas at a flow rate of 150 ml/min and with a heating rate of 65 °C/min. A weight of 5 mg of each sample was placed in the sample pan which was heated from 50 °C to 249 °C and held isothermally for 15 min at the latter temperature. The percentage of mass loss at the Noack reference time (t = 11.7 min) (Perkin Elmer, 2011), was determined for each sample run. Based on convenience, Noack volatility was measured for three levels of groundnut oil, POME and graphene nanoflakes. The discarded levels are 25 wt% and 75 wt% for groundnut oil, 5 vol% for POME and 0.1 wt% for graphene nanoflakes.

4. Statistical analysis

The numerical optimization was performed using the Design Expert software (version 7). Each parameter was assessed under the arrangement of full factorial design. A polynomial quadratic model such as the one shown in Eq (3) was generated for each parameter of interest. The models include quadratic, linear and interaction terms.

Table 3
Models statistical summary.

Parameter	Model F-Value	p-Value	R^2	Adjusted R^2	Predicted R^2	S/N Ratio
SR	33.48	<0.0001	0.8577	0.8321	0.8005	22
DV at $T = 40\,^{\circ}C$	1254.72	<0.0001	0.9938	0.9930	0.9919	125
VI	211.91	<0.0001	0.9646	0.9600	0.9537	50
TC	1390.47	<0.0001	0.9944	0.9937	0.9924	109
NV	3736.80	<0.0001	0.9995	0.9992	0.9986	149

$$f = \beta_{11}\,G^2 + \beta_{22}\,P^2 + \beta_{33}\,Gr^2 + \beta_{12}\,G\,P + \beta_{13}\,G\,Gr + \beta_{23}\,P\,Gr + \beta_1\,G + \beta_2\,P + \beta_3\,Gr + \beta_0 \tag{3}$$

Where G is groundnut oil, P is POME and Gr is graphene. The constants β_{jj} where $j \neq 0$, represent quadratic coefficients for a single factor. On the other hand, the constants β_j where $j \neq 0$, are linear coefficients for a single factor. The interaction coefficient of two factors are represented by the coefficients β_{jn}, where $j \neq n$. The models were validated using the ANOVA analysis, predicted R^2, adjusted R^2 and signal to noise (S/N) ratio. The corresponding 3-D response surfaces of each model were also generated.

Multiple numerical optimizations were performed following desirability approach (Derringer and Suich, 1980). This approach works by calculating a desirability value which represents how desirable a particular solution is. Optimization was implemented under different constraints of independent and dependent variables. The factors that were optimized are the concentrations of groundnut oil, POME and graphene. The criteria of selection were based on maximization and minimization of the parameters of interest and not based on the target value. The desirability approach for the case of maximization and minimization for a single parameter are expressed as follows.

$$d = \begin{cases} 0 & y < L \\ \left(\dfrac{y-L}{U-L}\right)^r & L \le y \le U \\ 1 & y > U \end{cases} \tag{4}$$

$$d = \begin{cases} 1 & y < L \\ \left(\dfrac{U-y}{U-L}\right)^r & L \le y \le U \\ 0 & y > U \end{cases} \tag{5}$$

where d is the desirability, U is the upper limit, L is the lower limit, r is the shape of desirability function and y is the sample's response.

The multiple desirability functions can be used to calculate the desirability value for multiple responses. In this case, the optimum solution will be a tradeoff among the parameters of interest. The multiple desirability functions is calculated using Eq (6).

$$D = (d_1\,d_2\,d_3 \ldots d_m)^{1/m} \tag{6}$$

where D is the overall desirability and m represents the number of responses. Desirability d, assumes a value in the range of 0–1, with 1 being the most desirable and 0 being the least desirable.

5. Results and discussions

5.1. Model statistical analysis

The observed and recorded values of the parameters of interest are shown in Table 2. The terms DV, TC, VI, NV and SR refer to dynamic viscosity, thermal conductivity, viscosity index, Noack volatility and sedimentation rate respectively.

Table 3 shows the statistical summary of the fitted models. As it can be seen, all the models were found to satisfy statistical requirements. Thus, the p-value is less than 0.05 indicating that the model is significant. The R^2 value is very high which shows a good fitting and that the variability of the parameter of interest is well explained and predicted. The values of the adjusted and the predicted R^2, are in a close agreement which indicates that the models are not over-fitted with many predictors. The values of the S/N ratios are greater than 4 indicating adequate signals.

The generated models were further confirmed with the normal probability plot as shown in Fig. 1. It can be seen that the residuals of all the parameters examined follow approximately a straight line on the normal probability plot. This indicates that errors are normally and independently distributed which ensures that no structured variance that is not accounted for by the model is present.

5.2. Response of nanosuspension sedimentation rate

Figs. 2and 3 show the visual images of nanolubricant samples after sonication (day zero) and on the fourth day respectively. As it can be seen, the stability of the nanodispersion deteriorates with time. On the fourth day, sedimentation can be clearly distinguished as when compared to day zero. It can be observed that the nanosuspension stability increases with increasing the groundnut oil content. This can be the direct effect of the higher viscosity of the groundnut oil relative to the naphthenic base.

The sedimentation rate model is shown in Eq. (7). As shown in Fig. 4, the change of sedimentation rate with respect to POME follows parabolic shape. The sedimentation rate is maximum at about 3.5 vol% POME, meanwhile, the minimum value is achieved at the extremes of POME study region (0 vol% and 7 vol%). It can be deduced that the addition of POME to graphene nanolubricant results in interactional surface phenomena which achieve higher nanosuspension stability at the optimum concentration of POME. It is quite possible that graphene and POME form complex molecules that have higher nanosuspension stability at a particular concentration. Along the groundnut oil axis, the stability increases (lower sedimentation rate) with increasing groundnut oil concentration.

$$SR = -1.7499 \times 10^{-6}G^2 - 3.6372 \times 10^{-3}P^2 + 21.8698Gr^2 - 8.6202 \times 10^{-5}GP - 0.0108GGr - 0.03999PGr - 3.233 \times 10^{-3}G + 0.0392P + 2.9134Gr + 0.0592 \tag{7}$$

With respect to graphene, the sedimentation rate was found to increase with increasing the graphene nanoflakes concentration as

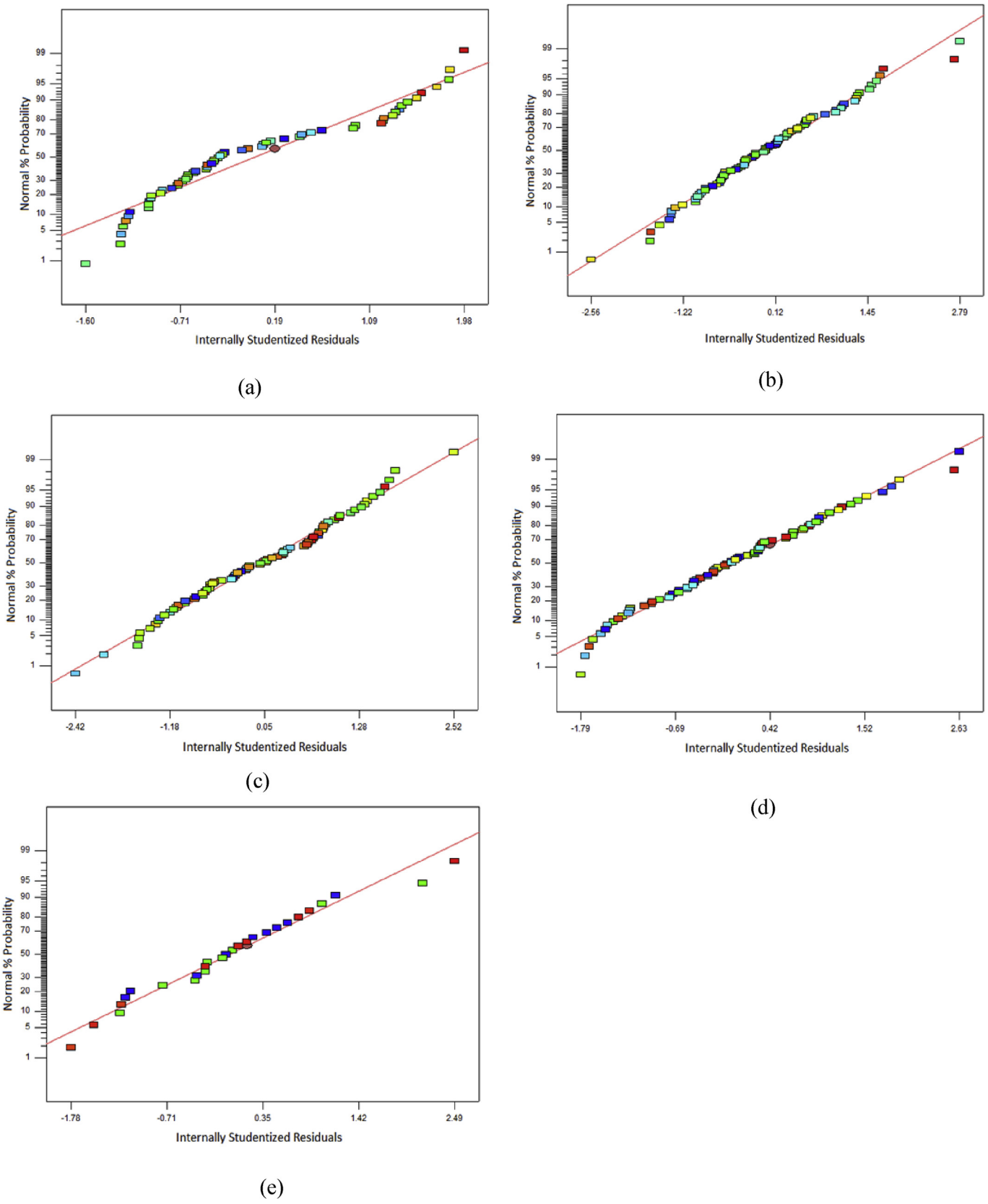

Fig. 1. Normal probability plot for (a) Sedimentation rate, (b) Dynamic viscosity, (c) Viscosity index, (d) Thermal conductivity, (e) Noack volatility.

shown in Fig. 4. The standard deviation for the results is presented in the supplement file. The decrease of the nanosuspension stability with graphene concentrations suggests that the likelihood of aggregation is increased for concentrated graphene samples. Aggregations result in the formation of heavier molecules which lowers liquid's inherent resistance to sedimentations and decreases nanosuspension stability. As a result, higher enhancement at higher concentrations of graphene might come at the cost of degrading nanosuspension stability. Therefore, a compromise between the achieved enhancements and the stability of the nanosuspension must be made. Furthermore, the effect of groundnut oil is not changed at the different level of graphene nanoflakes. Thus, the sedimentation rate is decreased with increasing groundnut oil concentration regardless of the weight fraction of graphene nanoflakes. Regarding the interaction effect between POME and graphene nanoflakes, 7 vol% of POME achieves the highest nanosuspension stability at different levels of graphene nanoflakes.

5.3. Response of dynamic viscosity

The dynamic viscosity model is shown in Eq. (8). As it can be seen from Fig. 5, the dynamic viscosity decreases with the addition of POME and increases with the addition of groundnut oil. The lower dynamic viscosity of POME relative to groundnut oil can be attributed to the transesterification process which reduces the viscosity of vegetable oils (Schuchardt et al., 1998). Since the film thickness is directly proportional to the absolute or dynamic viscosity (Stachowiak and Batchelor, 2006), it can be deduced that POME as an additive can be used to modify the viscosity which in turns modifies the film thickness. Additionally, it can be observed at higher levels of POME, the increase in dynamic viscosity by groundnut oil is smaller. This shows the presence of interaction between groundnut and POME. Furthermore, the higher dynamic viscosity of groundnut oil explains the reduction of the nanoflakes sedimentation rate as the concentration of groundnut oil is increased. This is because graphene nanoflakes have to overcome higher viscous forces in order to form agglomerates and sediment.

$$DV = 7.681 \times 10^{-4}G^2 + 0.026P^2 + 22.333Gr^2 - 1.861 \times 10^{-3}GP - 0.096GGr + 0.882PGr + 0.086G - 0.823P - 0.919Gr + 22.179 \quad (8)$$

The maximum reduction of dynamic viscosity by POME (22%) was achieved for the pure naphthenic lubricant at 7 vol% of POME. As the groundnut oil content is increased, the ability of POME to reduce dynamic viscosity becomes less significant. The maximum reduction of dynamic viscosity by POME for groundnut oil was found to be around 13% at 7 vol% of POME.

As it can be seen from Fig. 5, the change in dynamic viscosity with the increase of graphene nanoflakes is very small. This can be due to the small weight fractions used in this study. Higher enhancements may be found by increasing graphene's concentration. The effects of groundnut oil and POME are not changed at different levels of graphene nanoflakes. The achieved enhancements/reduction of dynamic viscosity in the presence of graphene nanoflakes are small. For instance, the relative change of dynamic viscosity for mineral oil is considerably lower (0.3% enhancement or 4 enhancement/wt at 0.075 wt%) than the maximum relative enhancement (61% increase or 122 enhancement/wt at 0.5 vol%) reported by Kumar et al. for Cu, Zn and Cu-Zn hybrid based vegetable oil nanofluid (Kumar et al., 2016). On the other hand, the relative reduction in dynamic viscosity of groundnut oil as a result of graphene nanoflakes addition is about 1.7% (23 reduction/wt at 0.075 wt%). The standard deviation for the results is presented in the supplement file.

5.4. Response of viscosity index

The viscosity index model is shown in Eq. (9). As it can be seen from Fig. 6, the viscosity index increases with increasing the content of groundnut oil and POME. The higher viscosity index of groundnut oil relative to the naphthenic base oil can be attributed to alicyclic nature of the latter and the presence of aromatic compounds (Rizvi, 2009). Similar to dynamic viscosity, the interaction between groundnut oil and POME is present. Thus, the increase of the viscosity index with the increase of groundnut oil content is larger at higher levels of POME. POME as an additive for viscosity index was found to be more effective with the naphthenic base than the groundnut oil. The highest enhancement of viscosity index by POME was achieved for the naphthenic base ($\approx$ 20% enhancement) at 7 vol%. Meanwhile, the maximum viscosity index enhancement for groundnut oil was found to be around 5% enhancement at 7 vol% of POME. The increase in viscosity index as result of POME addition can be attributed to the ester fatty acids present in POME. However, due to the chemical similarity between POME and groundnut oil, the enhancement of viscosity index enhancement of groundnut oil by POME is less effective when compared to that of the naphthenic base. The relative enhancement of viscosity index for diesel fuel blended with POME as computed from the reported data of Belyamin et al. (2013), was found to be lower than the ones reported in this study.

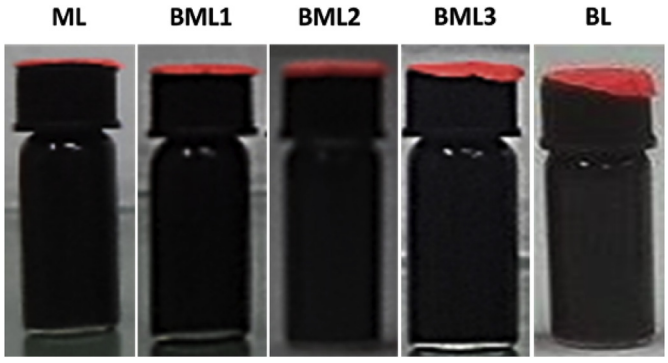

Fig. 2. Stability of nanolubricant samples immediately after sonication.

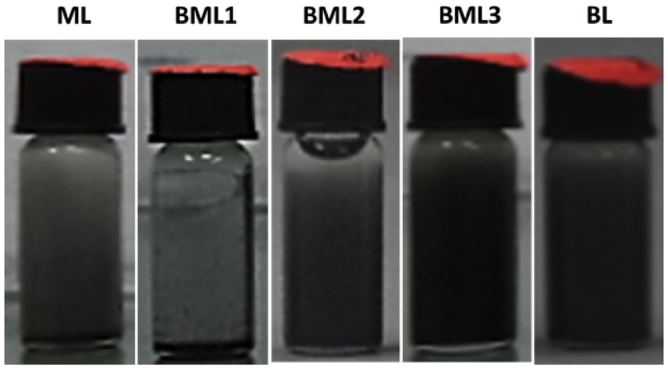

Fig. 3. Stability of nanolubricant samples on the fourth day.

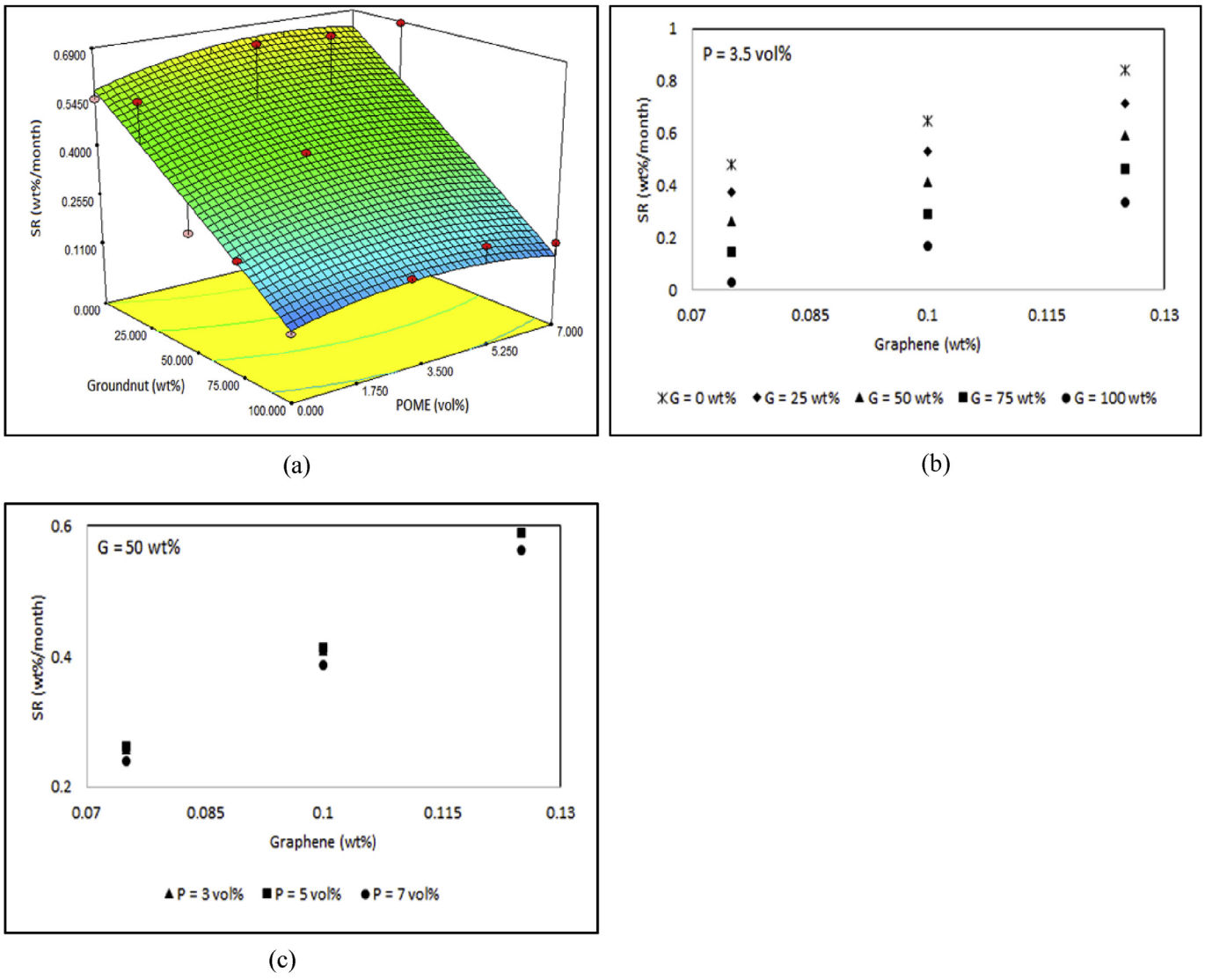

Fig. 4. (a) Response surface of sedimentation rate showing the interaction of groundnut oil and POME, (b) Interaction effect of groundnut oil and graphene nanoflakes, (c) POME and graphene nanoflakes.

$$VI = -3.996 \times 10^{-3}G^2 - 0.073P^2 - 685.179Gr^2 - 0.031GP + 0.305GGr - 4.112PGr + 1.274G + 5.511P + 129.512Gr + 179.068 \quad (9)$$

Similar to dynamic viscosity, the effect of graphene nanoflakes on viscosity index is relatively small. As it can be observed from Fig. 6, the viscosity index generally decreases with the increase of graphene nanoflakes. However, as the groundnut oil concentration is increased, graphene nanoflakes at 0.1 wt% achieves the lowest viscosity index. On the contrary, graphene nanoflakes at 0.1 wt% achieve the highest viscosity index when POME is added. The enhancement in the viscosity index of groundnut oil with the addition of 0.125 wt% graphene nanoflakes is around 3.5%. Relative to this, the enhancement achieved by graphene nanoflakes for the viscosity index of the naphthenic base at the same weight fraction is slightly lower (3.1% enhancement).

5.5. Response of thermal conductivity

Thermal conductivity is an important parameter to assess the heating effect and cooling characteristics of the lubricants. The thermal conductivity model is shown in Eq. (10). Analysis of the thermal conductivity as it can be observed in Fig. 7 shows that the thermal conductivity increases with increasing groundnut oil weight fraction. This indicates that the thermal conductivity of groundnut oil is higher than that of the naphthenic base oil. This behavior can be explained by referring to the Andrade's theory (Mohanty, 1951), which is based on treating liquid molecules as executing vibrations similar to that of solid state. The generated model shows that the thermal conductivity is directly proportional to the liquid's viscosity. By referring to this model, groundnut oil has higher viscosity and therefore it has higher thermal conductivity relative to the naphthenic base. The response surface of thermal conductivity as a function of groundnut oil and POME concentrations is a flat surface which decreases along the groundnut oil axis. Showing that the effect of POME on thermal

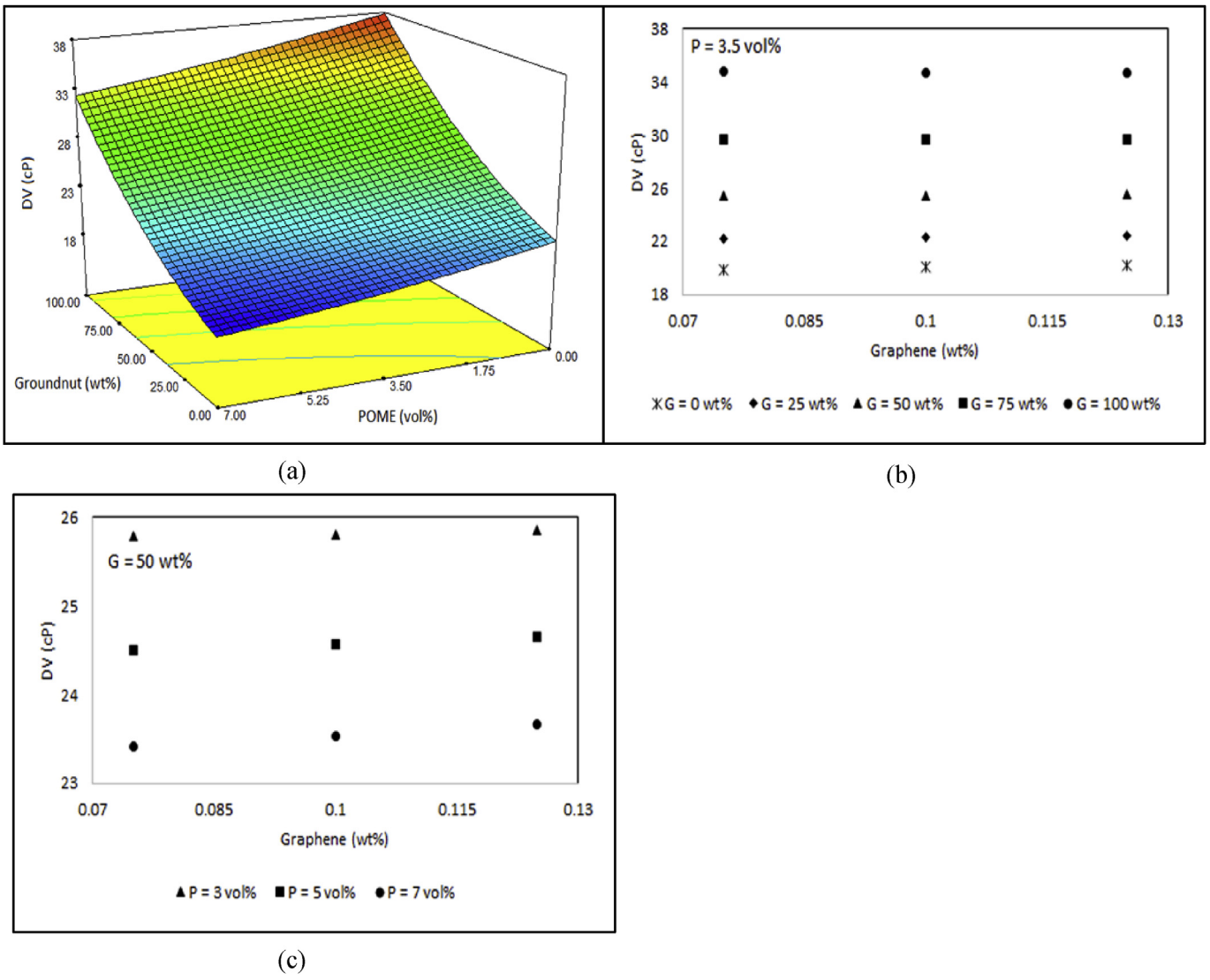

Fig. 5. (a) Response surface of dynamic viscosity showing the interaction of groundnut oil and POME, (b) Interaction effect of groundnut oil and graphene nanoflakes, (c) POME and graphene nanoflakes.

conductivity is insignificant. This can be noted from Eq. (10) where the quadratic and linear coefficients of POME are comparable to that of groundnut oil. Thus, in order for POME to cause a significant change in thermal conductivity, it must be added at higher amounts. Although low enhancement, POME on increases the thermal conductivity.

$$TC = 3.412 \times 10^{-7}G^2 + 1.179 \times 10^{-5}P^2 + 0.065Gr^2 - 4.857 \times 10^{-6}GP - 5.429 \times 10^{-6}GGr - 1.744 \times 10^{-3}PGr + 4.095 \times 10^{-4}G + 3.202 \times 10^{-4}P + 7.293 \times 10^{-3}Gr + 0.1155 \quad (10)$$

Similar to POME, the effect of graphene nanoflakes on thermal conductivity is very small. The thermal conductivity increases with increasing graphene nanoflakes concentration but at the very small rate. Fig. 7 shows the presence of interaction between POME and graphene nanoflakes. At weight percentage of 0.075 of graphene nanoflakes, the thermal conductivity increases with increasing the volume fraction of POME. However, as the graphene nanoflakes weight fraction is increased, a lower concentration of POME results in higher thermal conductivity. The increase of thermal conductivity by graphene can be attributed to the random motion of nanoflakes. At higher concentrations of graphene, the effect of random motion is more likely to become more significant which can results in higher enhancements when compared to the enhancements recorded from this study.

Although the enhancement is quite small, thermal conductivity enhancements by graphene nanoflakes are higher to that of conventional micro-sized particles in terms of recorded enhancement relative to the weight fraction added. Lee et al., reported that the maximum thermal conductivity enhancements achieved by conventional particle liquid-suspension are 40% at 10% concentration of particles (4 enhancement/wt) (Lee et al., 2010). From this study, the thermal conductivity enhancement for POME-free samples were found to be in the range of 1.2%–1.7% at 0.125% weight percentage of graphene (9.6–13.6 enhancement/wt). Singh et al., reported thermal conductivity enhancements of about 3.48% for hybrid alumina-graphene nano-cutting fluid at a concentration of

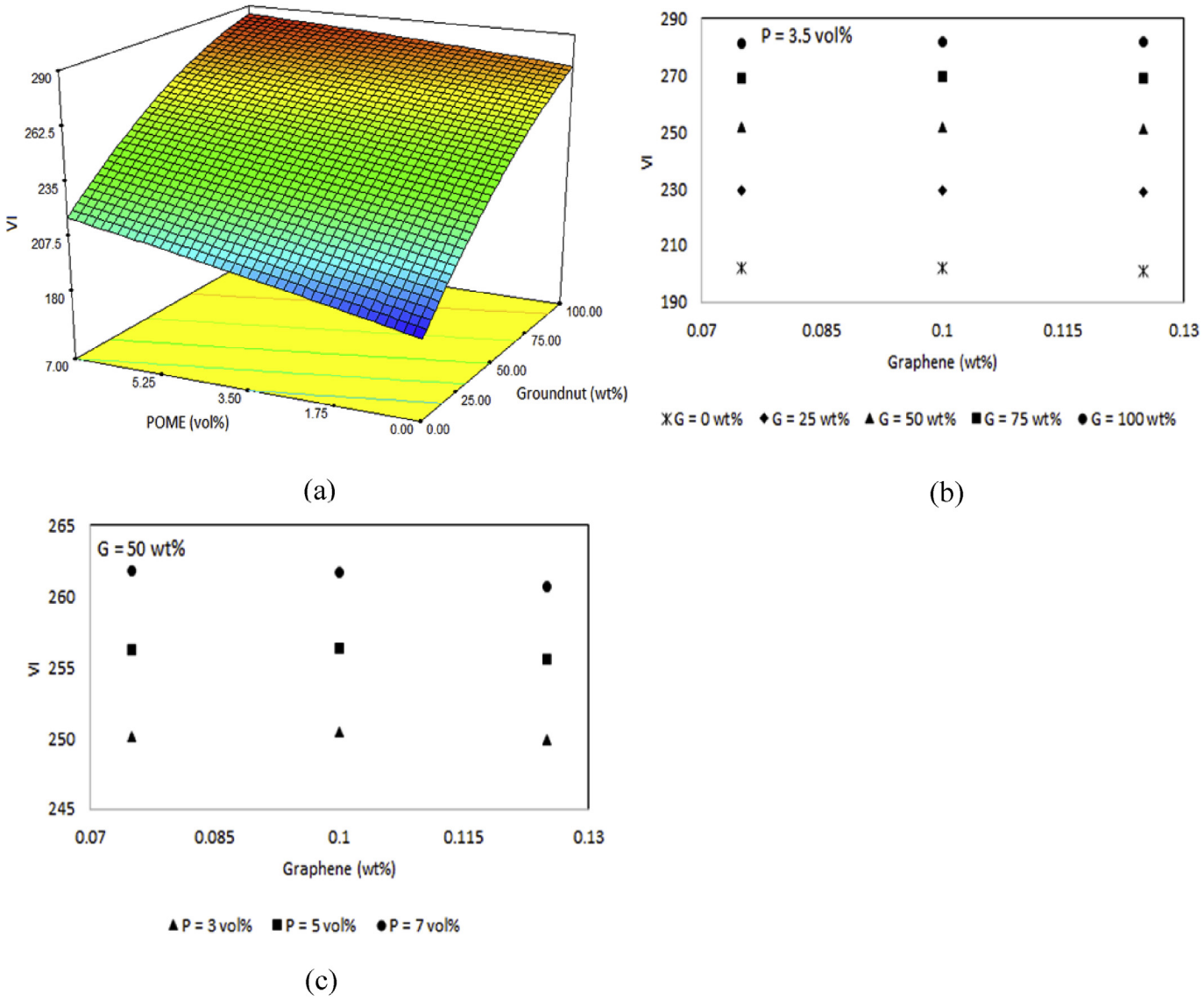

Fig. 6. (a) Response surface of viscosity index showing the interaction of groundnut oil and POME, (b) Interaction effect of groundnut oil and graphene nanoflakes, (c) POME and graphene nanoflakes.

0.25 vol% (Singh et al., 2017). The reported enhancements of hybrid alumina-graphene nanoflakes are higher to the reported enhancements from this study, however, at relatively higher concentration. Relative to MoS_2 nanoparticles with enhancement of 3.1% (3 enhancement/wt) in vegetable oils (Padmini et al., 2016), graphene nanoflakes from this study prove to be superior. Graphene nanoflakes from this study had comparable performance to that of copper-based kerosene nanofluid (Li et al., 2011). Nevertheless hybrid Cu-Zn based vegetable oil nanofluid shows higher thermal conductivity enhancement (48% or 96 enhancement/wt) (Kumar et al., 2016), in comparison to graphene nanoflakes from this study. The standard deviation for the thermal conductivity results is presented in the supplement file.

5.6. Response of Noack volatility

The Noack volatility model is shown in Eq (11). As it can be seen from Fig. 8, volatility decreases with increasing groundnut oil content. Thus, groundnut oil has significantly lower volatility when compared to the naphthenic base. This can be attributed to the polar nature of groundnut oil (Rizvi, 2009). In this study, the naphthenic base has a Noack volatility of about 95%. This result is not very different from the reported volatility of naphthenic base (98.8%) (Sharma et al., 2008), in the literature. On the other hand, volatility increases with increasing POME concentration for all the samples except for pure naphthenic base oil. The increase of volatility by POME in the presence of groundnut oil can be attributed to the transesterification process which increases the volatility of vegetable oils (Schuchardt et al., 1998). This can also be viewed from Eq (11) in which groundnut-POME interaction term has a positive coefficient. In contrast, for the pure naphthenic base, addition of POME imparts ester molecules to the mixture which helps to reduce the volatility (Rizvi, 2009).

$$NV = 3.829 \times 10^{-4}G^2 + 0.0345P^2 - 315.234Gr^2 + 8.473 \times 10^{-3}GP - 0.33GGr - 0.18PGr - 0.97G - 0.302P + 66.878Gr + 94.688 \quad (11)$$

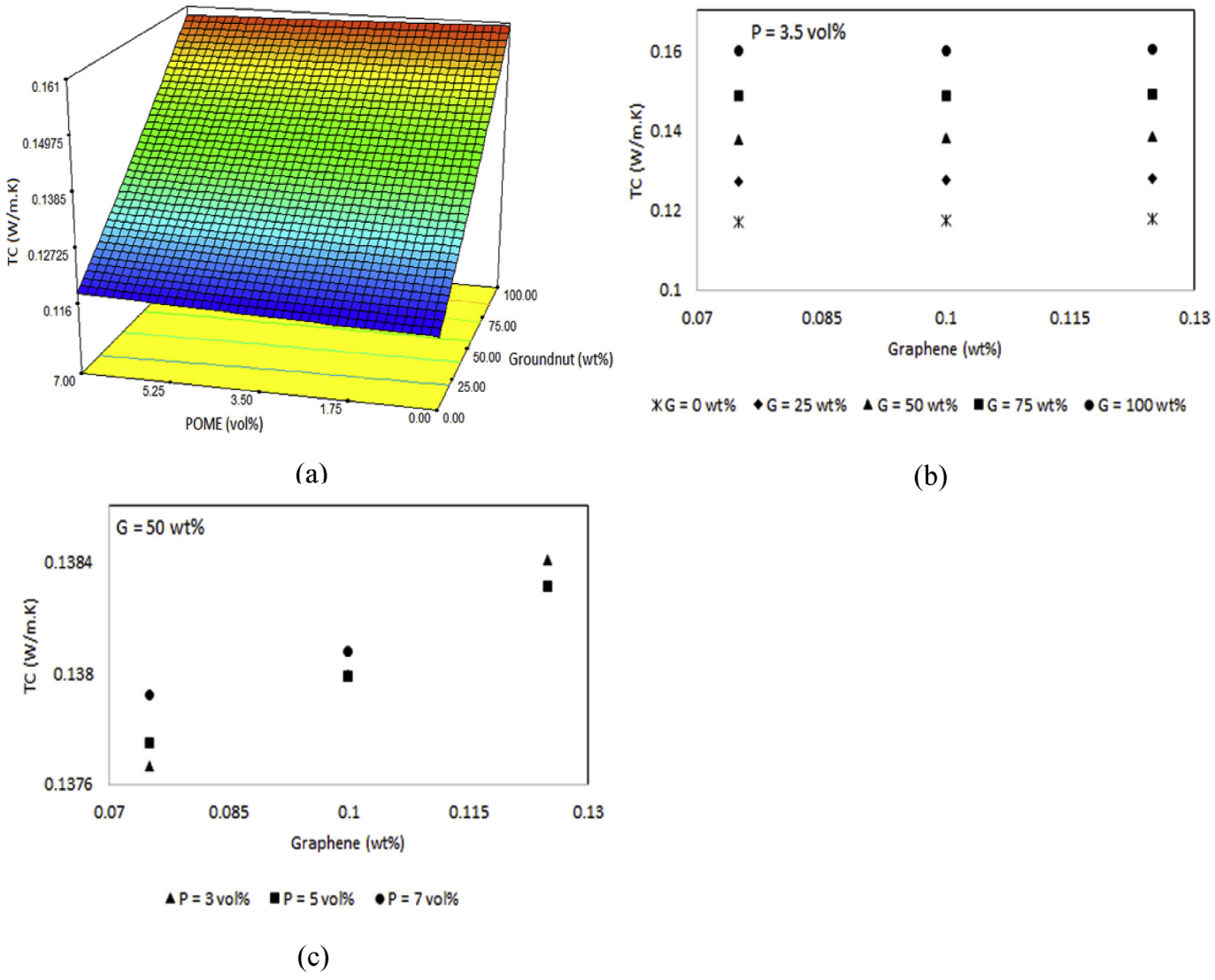

Fig. 7. (a) Response surface of thermal conductivity showing the interaction of groundnut oil and POME, (b) Interaction effect of groundnut oil and graphene nanoflakes, (c) POME and graphene nanoflakes.

The behavior of the volatility as a function of groundnut oil is opposite to that of the dynamic viscosity. Thus, as groundnut oil increases, dynamic viscosity increases and volatility decreases. The contradicted behavior can be explained by examining the change of molecular forces as the temperature is changed. Viscosity at the molecular level can be due to molecular forces, size of liquid molecules and molecular arrangement (Munson et al., 2009). At high temperatures, liquid molecules gain energy which reduces molecular forces. This is, in turn, helps to reduce viscosity and at large values it causes the molecules to escape by mean of evaporation. Thus, higher viscosity indicates higher molecular forces which in turn suppresses volatility.

As it can be seen from Fig. 8, at high levels of groundnut oil, volatility decreases with increasing graphene nanoflakes weight fraction. In contrast, at low levels of groundnut oil, 0.1 wt% of graphene nanoflakes achieves the highest volatility. Besides, volatility reduces with increasing graphene nanoflakes concertation regardless of the POME level as shown in Fig. 8.

5.7. Numerical optimization

Numerical optimization was performed following the desirability approach. The single response was optimized by calculating the desirability value using either Eq. (4) or (5) for maximization or minimization of response respectively. For example, in order to optimize the dynamic viscosity for the maximum value, Eq. (4) is used to calculate the desirability value. The lower and upper limits (L and U respectively) are set based on the maximum and minimum responses for a particular response region of interest. The term y in Eqs. (4) and (5) represent the response value for a particular sample. For instance, the values of y were calculated for the dynamic viscosity following Eq. (8). For the cases of multiple response optimization, the desirability values of individual responses are firstly calculated using Eqs. (4) and (5), then the multiple response desirability value is calculated using Eq. (6) by inserting the values of single response desirability.

In Table 4, optimization solutions for different cases of

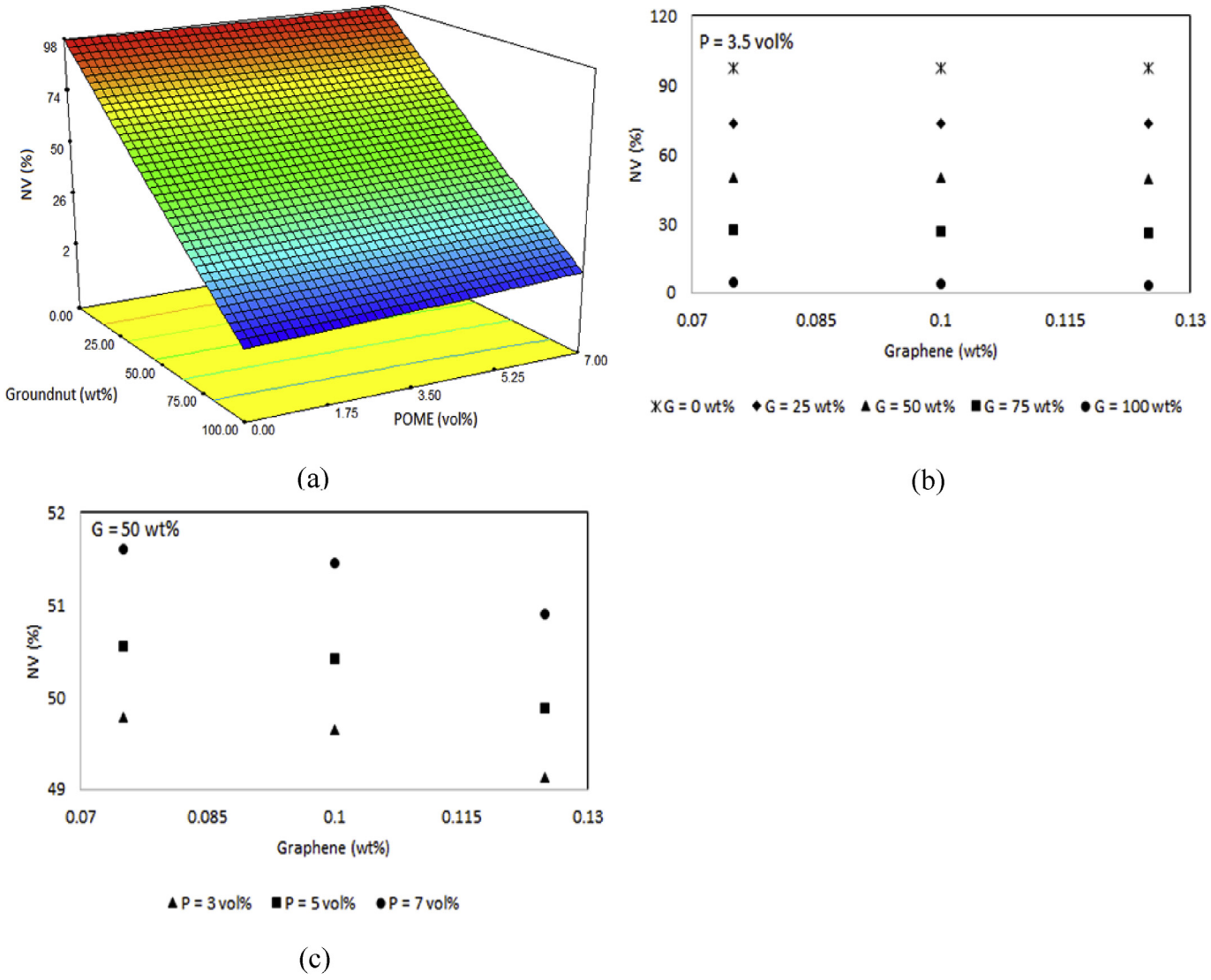

Fig. 8. (a) Response surface of Noack volatility showing the interaction of groundnut oil and POME, (b) Interaction effect of groundnut oil and graphene nanoflakes, (c) POME and graphene nanoflakes.

Table 4
Optimized parameters for different cases.

		Optimum Solutions				
Desired Responses	Fluid Type	N (wt%)	G (wt%)	P (vol%)	Gr (wt%)	Desirability
Max DV	Basefluid	0	100	0	0	0.995
	Nanolubricant	0	100	0	0.075	0.962
Max DV, Max TC	Basefluid	0	100	0	0	0.974
	Nanolubricant	0	100	0	0.118	0.970
Max DV, Max TC	Basefluid	0	100	0	0	0.943
Max VI, Min NV, Min SR	Nanolubricant	0	99.5	0	0.075	0.953

individual and multiple responses optimizations are shown. The terms N, G, P and Gr stand for naphthenic, groundnut, POME and graphene respectively. As it can be seen, all the conditions examined favor pure groundnut oil content. Alternative solutions are possible by using different criteria such as minimum dynamic viscosity, minimum viscosity index or target response value. Under these conditions, blend composition is more likely to be the optimum solution.

6. Conclusion

In this study, the thermophysical properties of bio-mineral lubricants and graphene nanolubricants were measured and modeled. Based on the models generated, optimization was carried out. From the experiments, we conclude the following.

1. Groundnut oil has better temperature dependent viscosity, thermal cooling and volatility characteristics when compared to naphthenic base oil.

2. POME as an additive was found to be more effective when added to naphthenic base oil as compared to groundnut oil. This can be proven by noting the higher enhancements/reductions in dynamic viscosity (20% reduction), viscosity index (20%) and volatility of naphthenic base oil as a result of POME inclusion.
3. The stability of graphene nanolubricant was found to decrease with increasing its concentration and increasing naphthenic base composition. Furthermore, graphene was found to result in enhancements of dynamic viscosity (3.2%), viscosity index (1.9%–3.5%) and thermal conductivity (1.2%–1.7%) at low concentrations. Additionally, graphene nanoflakes were generally found to reduce the volatility.
4. Groundnut oil has excellent thermophysical properties relative to the naphthenic base. POME and graphene nanoflakes can be used to enhance viscosity-temperature properties and volatility.

These findings reveal the potential of groundnut oil, POME and graphene nanoflakes for metalworking and industrial applications. In future, optimization can be performed by considering the desired lubricating performance (groundnut oil, POME, graphene or graphene-POME). The relative importance of each parameter considered must be determined in relation to industrial requirements. Consequently, the optimization performed can lead to the selection of feasible and economical samples that can be commercialized. Other properties that can be included in the optimization process are tribological characteristics such as wear rate, frictional coefficient, surface roughness, etc.

Acknowledgments

The authors acknowledge ExcelVite Sdn. Bhd. and Nynas Pte. Ltd. for providing POME and naphthenic base oil for this research.

Appendix A. Supplementary data

Supplementary data related to this article can be found at https://doi.org/10.1016/j.jclepro.2018.05.070.

References

D'Agostino, V., Senatore, A., Petrone, V., Ciambelli, P., Sarno, M. Tribological behaviour of graphene nanosheets as lubricant additive. In: Proceeding of the 15th International Conference on Experimental Mechanics ICEM15, Porto, Portugal, July 22-27, 2012.
Belyamin, Belyamin, Noor, A.B.M., Hussein, M.H., 2013. Characterization of Palm Oil Methyl Esther Used on Diesel Engine at Different Compression Ratio, Presented at 6th International Conference on Process Systems Engineering 2013, pp. 618–623.
Berman, D., Erdemir, A., Sumant, A.V., 2014. Graphene: a new emerging lubricant. Mat. Tday 17, 31–42.
Chang, H., Lo, C.H., Tsung, T.T., Cho, Y.Y., Tien, D.C., Chen, Liang Chia, Thai, C.H., 2005. Temperature effect on the stability of CuO nanofluids based on measured particle distribution. Key Eng. Mater. 295–296, 51–56.
Chen, M., Qin, X., Zeng, G., 2017. Biodegradation of carbon nanotubes, graphene, and their derivatives. Trend. Bio. Tech 35, 836–846.
Dayou, S., Liew, W.Y.H., Ismail, M.A.B., Dayou, J., 2011. Evaluation of palm oil methyl ester as lubricant additive using milling and four-ball tests. Int. J. Mech. Mater. Eng. 6, 374–379.
Derringer, G., Suich, R., 1980. Simultaneous optimization of several response variables. J. Qual. Technol. 12, 214–219.
Do, The-Vinh, Hsu, Quang-Cherng, 2016. Optimization of minimum quantity lubricant conditions and cutting parameters in hard milling of AISI H13 steel. Appl. Sci. 83, 1–11.
Groover, M.P., 2010. Fundamentals of Modern Manufacturing Materials, Processes, and Systems. JOHN WILEY & SONS, INC., United States of America.
Han, Haoxue, Zhang, Yong, Wang, Nan, Samani, Majid Kabiri, Ni, Yuxiang, Mijbil, Zainelabideen Y., Edwards, Michael, Xiong, Shiyun, Sääskilahti, Kimmo, Murugesan, Murali, Fu, Yifeng, Ye, Lilei, Sadeghi, Hatef, Bailey, Steven, Kosevich, Yuriy A., Lambert, Colin J., Liu, Johan, Volz, Sebastian, 2016. Functionalization mediates heat transport in graphene nanoflakes. Nat. Commun. 7, 11281.
Joseph, M.P., Leslie, R.R., Sevim, Z.E., 2013. Natural oils as lubricants. In: Heinemann, H. (Ed.), Synthetics, Mineral Oils, and Bio-based Lubricants. CRC Press, pp. 375–384.
Khalid, K., Khalid, K., 2011. Transesterification of palm oil for the production of biodiesel. Am. J. Appl. Sci. 8, 804–809.
Kumar, M.S., Vasu, V., Gopal, A.V., 2016. Thermal conductivity and viscosity of vegetable oil–based Cu, Zn, and Cu–Zn hybrid nanofluids. J. Test. Eval. 44, 1077–1083.
Kuram, E., Simsek, B.T., Ozcelik, B., Demirbas, E., Askin, S., 2010. Optimization of the Cutting Fluids and Parameters Using Taguchi and ANOVA in Milling, Presented at the World Congress on Engineering 2010. Imperial College London, London, U.K.
Lawal, S.A., Abolarin, M.S., Ugheoke, B.I., Onche, E.O., 2007. Performance evaluation of cutting fluids developed from fixed oils. Leona. Elect. J. Pract. Tech.
Lawal, S.A., Choudhury, I.A., Nukman, Y., 2012. Application of vegetable oil-based metalworking fluids in machining ferrous metals—a review. Int. J. Mach. Tool Manufact. 52, 1–12.
Lee, Ji-Hwan, Lee, Seung-Hyun, Choi, C.J., Jang, S.P., Choi, S.U.S., 2010. A review of thermal conductivity data, mechanisms and models for nanofluids. Intl. J. Micr. Nana. Scal. Trans. 1, 269–322.
Li, Dan, Müller, Marc B., Gilje, Scott, Kaner, Richard B., Wallace, Gordon G., 2008. Processable aqueous dispersions of graphene nanosheets. Nat. Nanotechnol. 3, 101–105.
Li, D., Xie, W., Fang, W., 2011. Preparation and properties of copper-oil-based nanofluids. Nanosca. Res. Lett. 6, 373.
Lin, J., Wang, L., Chen, G., 2011. Modification of graphene platelets and their tribological properties as a lubricant additive. Tribol. Lett. 41, 209–215.
Mansot, J.L., Bercion, Y., Romana, L., 2008. Nanolubrication. Brazil. J. Physic 39.
Mohanty, R.S., 1951. A relationship between heat conductivity and viscosity of liquids. Nature 168, 42.
Muniz, C.A.S., Dantas, T.N.C., Moura, E.F., Neto, A.A.D., Gurgel, A., 2008. Novel formulations of cutting fluids using napthenic base oil. Brazil. J. Petrol. Gas. 2, 143–153.
Munson, B.R., Rothmayer, A.P., Okiishi, T.H., Huebsch, W.W., 2009. Fundamentals of Fluid Mechanics. John Wiley & Sons, Inc., United States of America.
Nurdin, Irwan, Ridwan, Satriananda, 2016. The effect of temperature on synthesis and stability of superparamagnetic maghemite nanoparticles suspension. J. Mater. Sci. Chem. Eng. 4, 35–41.
Ojolo, S.J., Amuda, M.O.H., Ogunmola, O.Y., Ononiwu, C.U., 2008. Experimental determination of the effect of some straight biological oils on cutting force during cylindrical turning. Mat. Rio. Janei 13, 650–663.
Padmini, R., Vamsi Krishna, P., Krishna Mohana Rao, G., 2016. Effectiveness of vegetable oil based nanofluids as potential cutting fluids in turning AISI 1040 steel. Tribol. Int. 94, 490–501.
Perkin Elmer, 2011. The TGA Noack test for the assessment of engine oil volatility. In: Application Note - Thermal Analysis. United States of America).
Pop, E., Varshney, V., Roy, A.K., 2012. Thermal properties of graphene: fundamentals and applications. MRS. Bullin 37, 1273–1281.
Rasheed, A.K., Khalid, M., Rashmi, W., Gupta, T.C.S.M., Chan, A., 2016. Graphene based nanofluids and nanolubricants – review of recent developments. Renew. Sustain. Energy Rev. 63, 346–362.
Rashmi, W., Ismail, A.F., Sopyan, I., Jameel, A.T., Yusof, F., Khalid, M., Mubarak, N.M., 2011. Stability and thermal conductivity enhancement of carbon nanotube nanofluid using gum Arabic. J. Exp. Nanosci. 6, 567–579.
Rashmi, W., Khalid, M., Lim, X.Y., GUPTA, T.C.S.M., ARWIN, G.Z., 2017. Tribological studies on graphene/TMP based nanolubricant. J. Eng. Sci. Technol. 12, 365–373.
Rizvi, S.Q.A., 2009. Comprehensive Review of Lubricant Chemistry, Technology, Selection, and Design. ASTM International.
Sadeghinezhad, Emad, Mehrali, Mohammad, Saidur, R., Mehrali, Mehdi, Latibari, Sara Tahan, Akhiani, Amir Reza, Metselaar, Hendrik Simon Cornelis, 2016. A comprehensive review on graphene nanofluids: recent research, development and applications. Energy Convers. Manag. 111, 466–487.
Schuchardt, U., Sercheli, R., Vargas, R.M., 1998. Transesterification of vegetable oils: a review. J. Braz. Chem. Soc. 9, 199–210.
Sharma, B.K., Adhvaryu, A., Perez, J.M., Erhan, S.Z., 2008. Effects of hydroprocessing on structure and properties of base oils using NMR. Fuel Process. Technol. 89, 984–991.
Singh, P.K., Sharma, A.K., Dixit, A.R., Tiwari, A.K., Parmanik, A., Mandal, A., 2017. Performance evaluation of alumina-graphene hybrid nano-cutting fluid in hard turning. J. Clean. Prod. 162, 830–845.
Sridhar, V., Lee, H.H., Chun, H.P., 2012. Graphene reinforced biodegradable poly(3-hydroxybutyrate-co-4-hydroxybutyrate) nano-composites. Poly. Lett. 7, 320–328.
Stachowiak, G.W., Batchelor, A.W., 2006. Physical properties of lubricants. In: Stachowiak, G.W., Batchelor, A.W. (Eds.), Engineering Tribology, third ed. Butterworth-Heinemann, pp. 11–50.
Thirumalraj, Balamurugan, Rajkumar, Chellakannu, Palanisamy, Shen-Ming Chen & Selvakumar, 2017. One-pot green synthesis of graphene nanosheets encapsulated gold nanoparticles for sensitive and selective detection of dopamine. Sci. Rep. 7, 41213.
Van Der Heide, E., Schipper, D.J., 2006. Friction and wear in lubricated sheet metal forming processes. In: Totten, G.E. (Ed.), Handbook of Lubrication and Tribology. CRC Press, pp. 28–35, 28–1.